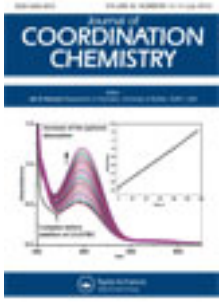

Journal of Coordination Chemistry
Publication details, including instructions for authors and subscription information:
http://www.tandfonline.com/loi/gcoo20

A thiocyanate-based hybrid molecular salt as a new fluorescent chemosensor for fluoride

Bhaskar Biswas [a], Shao-Po Hung [b], Hui-Lien Tsai [b], Rajarshi Ghosh [c] & Niranjan Kole [a]

[a] Department of Chemistry, Raghunathpur College, Purulia 723133, West Bengal, India

[b] Department of Chemistry, National Cheng Kung University, Tainan City 70101, Taiwan

[c] Department of Chemistry, The University of Burdwan, Burdwan 713104, West Bengal, India

Accepted author version posted online: 09 May 2012.Published online: 29 May 2012.

To cite this article: Bhaskar Biswas, Shao-Po Hung, Hui-Lien Tsai, Rajarshi Ghosh & Niranjan Kole (2012) A thiocyanate-based hybrid molecular salt as a new fluorescent chemosensor for fluoride, Journal of Coordination Chemistry, 65:13, 2280-2293, DOI: 10.1080/00958972.2012.692473

To link to this article: http://dx.doi.org/10.1080/00958972.2012.692473

Journal of Coordination Chemistry
Vol. 65, No. 13, 10 July 2012, 2280–2293

A thiocyanate-based hybrid molecular salt as a new fluorescent chemosensor for fluoride

BHASKAR BISWAS*†, SHAO-PO HUNG‡, HUI-LIEN TSAI‡, RAJARSHI GHOSH§ and NIRANJAN KOLE*†

†Department of Chemistry, Raghunathpur College, Purulia 723133, West Bengal, India
‡Department of Chemistry, National Cheng Kung University, Tainan City 70101, Taiwan
§Department of Chemistry, The University of Burdwan, Burdwan 713104, West Bengal, India

(*Received 20 December 2011; in final form 20 March 2012*)

An organic–inorganic hybrid solid $[(dpaH)^+(NCS)^-]$ (**1**) (dpa = 2,2′-dipyridylamine) based on an anionic template NCS^- has been synthesized. Single crystal X-ray structural analysis reveals that NCS^- templates assemble $dpaH^+$ units into a 3-D layer structure along the *b* axis through strong hydrogen bonding. Molecular salt **1** works as an anion-binder efficiently and selectively for recognition and sensing purposes in aprotic solvents. This receptor shows changes both in its UV-Vis absorption and fluorescence emission spectra upon the addition of F^-, resulting in high selectivity for fluoride detection in CH_3CN. It is promising to use these systems in various sensing applications.

Keywords: Synthesis; X-ray structure; Supramolecular coordination networks; Fluoride anion recognition

1. Introduction

Molecular architectures offer a route to encode the properties of materials at the molecular level. The development of anionic receptors has become a challenging area of research because of its importance for molecular recognition in biological systems as well as in supramolecular chemistry [1–6]. Crystal engineering [7] is based on the use of coordinate/covalent forces [8] together with one or more weaker forces such as hydrogen bonding [9], $\pi\cdots\pi$ interaction [10], C–H$\cdots\pi$ interaction [11], and other weak interactions such as metal–metal [12], S$\cdots$S [13], S$\cdots\pi$ [14] interactions, etc. Molecules containing NH fragments that behave as anion-binding motifs are widely used as receptors for recognition and sensing in aprotic solvents. 2,2′-Dipyridylamine is weakly luminescent and this is retained in some of its complexes. Typical examples are neutral charge receptors containing pyrrole, amide, indolocarbazole, guanidium, imidazolium, and urea/thiourea moieties. Polyamines like dipyridylamine and its derivatives [15] also

*Corresponding authors. Email: mr.bbiswas@rediffmail.com; niranjan12356@gmail.com

ISSN 0095-8972 print/ISSN 1029-0389 online
http://dx.doi.org/10.1080/00958972.2012.692473

have varying degrees of affinity and selectivity toward different anions such as F^-, $H_2PO_4^-$, etc. Though there are large numbers of pure covalent compounds and metal complexes available as fluorescent chemosensors, hybrid molecular salts containing uncommon anions are rare. Usually, anions are recognized *via* H-bonding, which is not easy to differentiate from the deprotonation of protons on the receptor –NH group [16]. The present endeavor deals with the designed synthesis of an organic–inorganic hybrid molecular salt, $[(dpaH)^+(NCS)^-]$ (**1**), whereby H-bonding between the protonated pyridine functional group (pyridinium) and the NCS anion allows the formation of an extended lattice. A further consequence of protonation of dpa is that the electronic properties are altered in such a way as to produce a luminescent compound; the absorption and luminescence properties are perturbed to various degrees by a variety of anions, with the most striking effect seen for fluoride in the MeCN solution.

2. Experimental

2.1. *Preparation of the complex*

2.1.1. Chemicals, solvents, and starting materials. High purity 2,2′-dipyridylamine (dpa) (Fluka, Frankfurt, Germany), ammonium thiocyanate (E. Merck, Mumbai, India), tertiary butyl ammonium salts (Aldrich, Manchester, UK), and all reagents were purchased and used as received.

2.1.2. General synthesis of 1. The molecular salt **1** was prepared by the reaction of dpa with ammonium thiocyanate by the addition of 20% HCl or lanthanide ions (La^{3+}, Gd^{3+}, Dy^{3+}, Tb^{3+}, or Eu^{3+}) at room temperature in the methanol–dimethylformamide (DMF) solution (scheme 1). Colorless crystals suitable for X-ray data collection were obtained by slow evaporation of the resultant reaction mixture. The different formulations were confirmed by elemental analysis, crystallographic diffraction, and spectroscopic measurements.

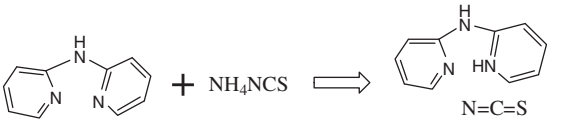

Scheme 1. Preparative procedure of the salt **1**.

2.2. *Physical measurements*

Elemental analyses (carbon, hydrogen, and nitrogen) were performed on a Perkin Elmer 2400 CHNS/O elemental analyzer. IR spectra were recorded (KBr discs, 4000–300 cm^{-1}) using a Perkin Elmer RX1 FTIR spectrometer. Ground state

Table 1. Crystallographic data and crystal parameters of $C_{11}H_{10}N_4S$ (**1**).

Empirical formula	$C_{11}H_{10}N_4S$
Formula weight	230.30
Temperature (K)	200(2)
Wavelength (Å)	0.71073
Crystal system	Monoclinic
Space group	$P2_1/c$
Unit cell dimensions (Å, °)	
a	9.349(3)
b	12.720(4)
c	9.530(3)
α	90
β	102.665(4)
γ	90
Volume (Å^3), Z	1105.6(6), 4
Calculated density (Mg m^{-3})	1.383
Absorption coefficient (mm^{-1})	0.269
$F(000)$	480
Crystal size (mm^3)	$0.51 \times 0.35 \times 0.22$
θ range for data collection (°)	2.23–28.30
Limiting indices	$-12 \le h \le 12$, $-16 \le k \le 15$, $-12 \le l \le 12$
Reflections collected	7805
Independent reflections	2710 [R(int) = 0.0392]
Completeness to $\theta = 28.30$ (%)	98.4
Max. and min. transmission	0.943 and 0.893
Refinement method	Full-matrix least-squares on F^2
Data/restraints/parameters	2710/0/145
Goodness-of-fit on F^2	1.200
Final R indices [$I > 2\sigma(I)$]	$R_1 = 0.0786$, $wR_2 = 0.2835$
R indices (all data)	$R_1 = 0.0886$, $wR_2 = 0.2910$
Largest difference peak and hole (e Å^{-3})	0.455 and −0.287

absorption was measured with a JASCO V-530 UV-Vis spectrophotometer. The fluorescence spectra were recorded on the Fluorometer Hitachi-2000.

2.3. *X-ray diffraction study*

Crystal diffraction data were measured using a Bruker SMART APEX II CCD diffractometer. The data were collected with graphite monochromated Mo-Kα radiation ($\lambda = 0.71073$ Å) at 200 K. The structure was resolved by direct methods and refined by full-matrix least-squares using the SHELXL-97 software package [17, 18]. The crystallographic data are summarized in table 1.

2.4. *Spectroscopic measurements*

There are differences between the salt and free ligand in the IR spectrum. In **1**, the dpa shows N–H stretch at 3421 cm^{-1}. In this region the position of the vibration largely depends on the extent of hydrogen bonding. These vibrations shift to lower frequency (longer wavelengths) with band widening in the salt as compared to free dpa. Also, well-resolved peaks are observed at 2052 and 1583 cm^{-1} attributed to ν(NCS) and ν(C=N) stretching modes, respectively [19]. Weak bands at 2980–2900 cm^{-1} are assignable to

aliphatic C–H stretching. UV-Vis absorption spectra of **1** in CH_3CN solution were recorded from 200 to 900 nm. The salt displays intense absorptions in CH_3CN at 262 and 308 nm which are assignable to n–π^* and π–π^* transitions of –C=N of pyridyl rings of protonated dpa [20].

2.5. *Anion sensing experiments*

The spectral analyses display an excellent chemosensory response in both the absorption and fluorescence of **1** upon the addition of trace amounts of fluoride in acetonitrile (ACN). The selectivity of receptor **1** for F^- over other anions was studied in detail. Variations in the UV-Vis absorption spectra and fluorescence spectra of **1** in ACN in the presence of anions such as F^-, Cl^-, Br^-, $H_2PO_4^-$, and AcO^- are shown in the "Supplementary material," respectively.

2.6. *Optimization study*

The optimized structural parameters of individual dpa, NH_4NCS, and their salt were calculated at B3LYP/6-31 G(d,p) basis sets.

3. Results and discussion

3.1. *Synthesis and formulation*

Hybrid salt **1** has been synthesized by the reaction of dpa with ammonium thiocyanate in the methanol–DMF solution at room temperature. The synthesis of **1** was carried out by dissolving dpa (1 mmol, 0.171 g) in 10 mL methanol : DMF (5 : 1, v/v) and lowering its pH to 4.8–5.2 by the dropwise addition of 20% HCl or 10^{-3} molL^{-1} concentrated methanolic solution of lanthanide ions (La^{3+}, Gd^{3+}, Dy^{3+}, Tb^{3+}, or Eu^{3+}) into the dpa solution. In a separate beaker, NH_4SCN (1 mmol, 0.076 g) was taken in 10 mL methanol and added slowly to the dpa reaction mixture with stirring. The resulting solution was left undisturbed at room temperature (scheme 1).

$$\text{dpa} + NH_4NCS \xrightarrow[\text{MeOH+DMF}]{20\%\text{HCl or } Ln^{3+}\text{ions}} [\text{dpaH}^+][NCS^-] \quad (1)$$

Colorless square-shaped crystals of **1** (128 mg, 75%) suitable for X-ray study appeared after 1 week. This was filtered and washed several times with hexane. The air-stable moisture-insensitive salt is soluble in all common solvents. Anal. Calcd for $C_{11}H_{10}N_4S$: C, 57.36; H, 4.37; N, 24.33. Found: C, 57.29; H, 4.41; N, 24.34. ν_{max} (cm^{-1}): 3421 s (NH), 2052 vs (NCS) and 1583 vs (CN). $\lambda_{max}(CH_3CN)$ (nm): 262, 308.

3.2. *Description of crystal structure*

The molecular salt **1** crystallizes in monoclinic with space group $P2_1/c$. The ORTEP diagram is shown in figure 1. The X-ray structure of **1** reveals the presence of four independent discrete $dpaH^+$ and four NCS^- in the unit cell bonded together through a

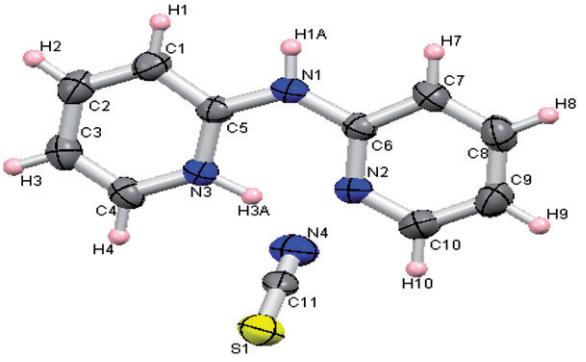

Figure 1. An ORTEP diagram of $[(dpaH)^{+}(NCS)^{-}]$ (**1**) with atom numbering scheme and 30% probability ellipsoids for all non-hydrogen atoms.

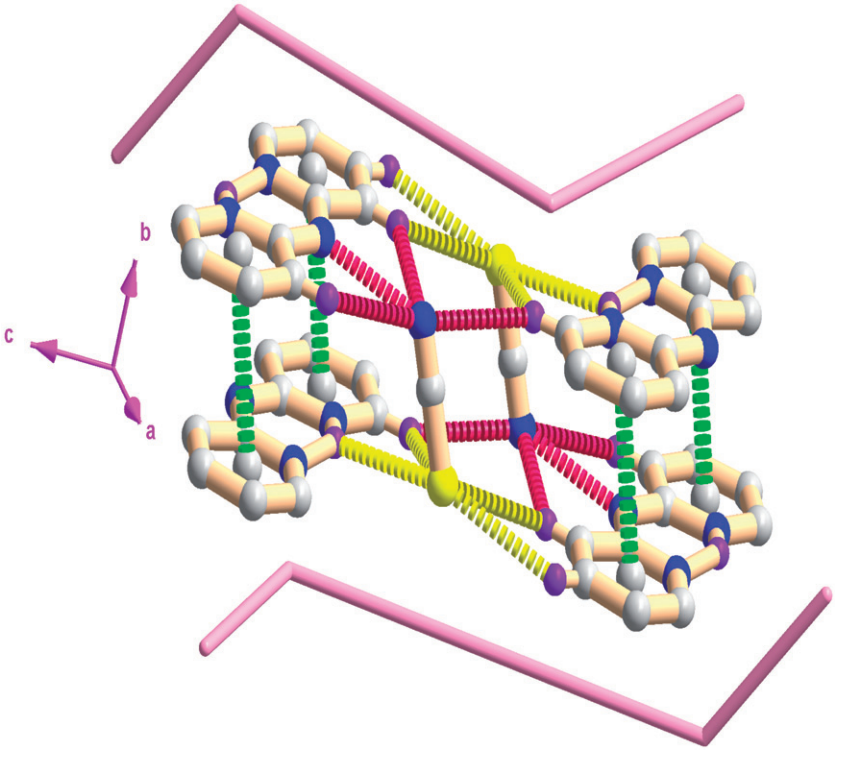

Figure 2. Perspective view of zigzag fashioned (4,4)-net topology of NCS^{-} in the dimer of **1**.

variety of hydrogen bonds and hybrid forces and forms a cationic–anionic pair. The geometry of thiocyanate is almost linear with an average bond angle of 179.9(5)° [∠S1–C11–N4, 179.9(5)°]. Protonation by one pyridine nitrogen in the acidic condition diminishes its chelating behavior. From X-ray diffraction it is clear that H3A

acceptance by the lone pair of N3 in one pyridine is very strong and that the acid–base interaction has occurred. It also revealed that after protonation the bond angles between amine N1 and pyridine N3 slightly differed. The bond angles are ∠N1C6N2 = 117.874° and ∠N1C5N3 = 120.304°. The crystallographic parameters are provided in table 1.

3.3. *Driving forces for directed assembly*

Linear NCS^- centers act as end-to-end bridging template for (4,4) coordination networks (figure 2) and by using different weak molecular forces it organizes $dpaH^+$ into a thick 2-D supramolecular sheet (figure 3). The organizing $dpaH^+$ by NCS^- are grown in a zigzag fashion (figure 2) and assemble in a columnar molecular packing. The sheet is the (010) plane in which each NCS^- is a node and connects other nodes through $dpaH^+$ bridges mediated by hydrogen-bonding interactions (table 2). Though mainly C/N–H···N and C/N–H+···S hydrogen-bonding determines the network structure, there are important N···π, S···π, π···π and N···N short contacts in the supramolecular assembly of the sheet in a columnar packing (figure 4). The successive thick 2-D sheets pack in an ABAB fashion, in which the nodes of the B layer overlay the grid center of the A layer debarring possible channel space. Due to the availability of pyridyl π

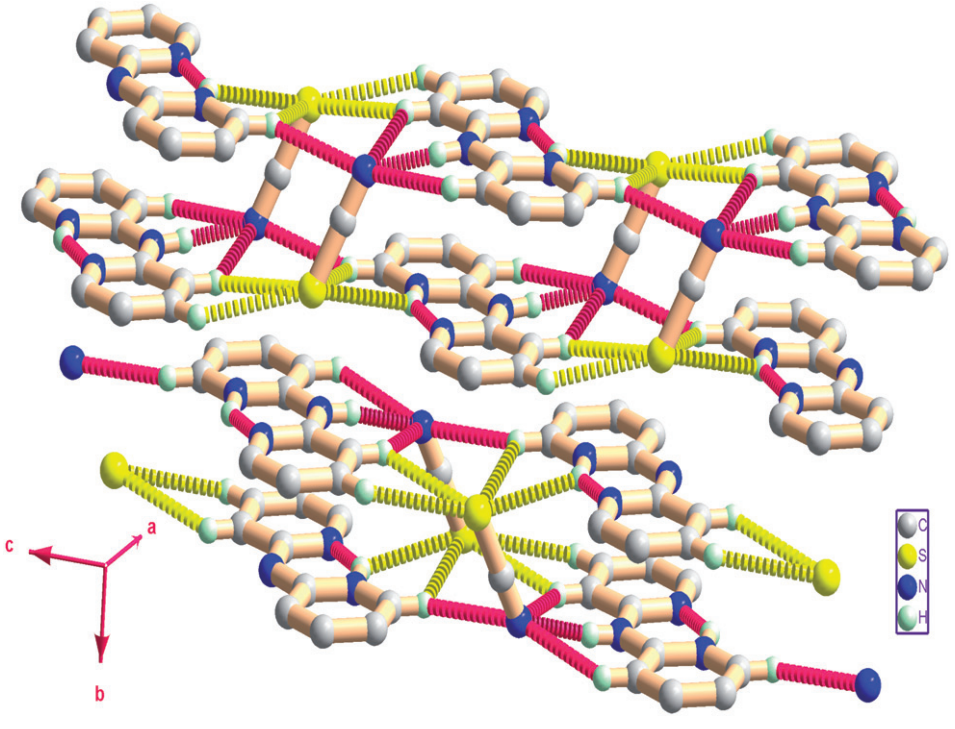

Figure 3. SCN^- templates assembling 2-D columnar structure in **1** by organizing $dpaH^+$ molecules through inter- and intramolecular hydrogen bonds (red dotted bond implies the intra/intermolecular H-bond between N and H and yellow dotted bond implies the intermolecular H-bond between S and H).

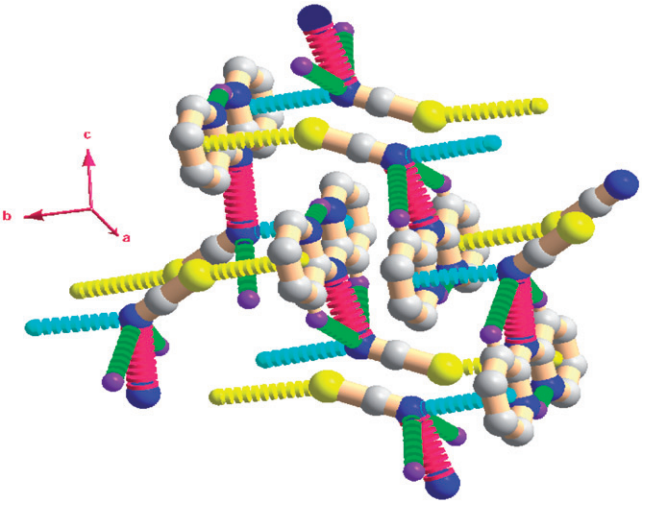

Figure 4. Schematic representation of 3-D parallel interpenetration *via* N···N interaction with N···H, S···π, and N···π interactions along the *c* axis (red = N···N, cyan = N···π, yellow = S···π and green = N···H interactions).

interaction sites, the $dpaH^+$ ions align optimally to facilitate $\pi\cdots\pi$ interactions

Table 2. Geometrical parameters of C/N–H···N and C/N–H···S hydrogen bonds (Å, °) involved in the supramolecular construction in **1**.

Compound	D–H···A	D–H	H···A	D···A	D–H···A
1	N(1)–H(1A)···N(4)[a]	0.89(5)	1.97(5)	2.849(5)	169(4)
	C(1)–H(1)···N(4)[a]	0.93(6)	2.931	3.584	137.89
	C(4)–H(4)···N(4)[b]	0.93(6)	2.891	3.635(5)	128.43
	C(7)–H(7)···N(4)[a]	0.93(6)	2.904	3.567	128.66
	N(3)–H(3A)···N(2)[a]	0.99(7)	1.76(7)	2.617(4)	143(6)
	N(3)–H(3A)···S(1)[c]	0.99(7)	2.936(7)	3.542	120
	C(4)–H(4)···S(1)[c]	0.93(6)	3.070	3.648	122
	C(7)–H(7)···S(1)[d]	0.93(6)	3.031	3.683	116
	C(8)–H(8)···S(1)[d]	0.93(6)	3.143(7)	3.748	124.4

$\pi\cdots\pi$ Interactions (Å, °) for **1**

Cg–Cg	Cg–Cg distance	Dihedral angle (*i*,*j*)	Perpendicular distance
Cg1···Cg2[e]	3.669(3)	1.70(19)	3.4342(18)
Cg2···Cg1[e]	3.669(3)	1.70(19)	3.4341(17)

N···π and S···π interactions (Å, °) for **1**

Y–X···Cg	X···Cg distance	∠Y–X···Cg
C11–S1···Cg1[f]	3.569(2)	154.08(13)
C11–N4···Cg2[g]	3.325(4)	147.7(3)
N4···N1 interaction[h]	2.849 Å	

D = donor, A = acceptor (Å, °).
Symmetry transformations used to generate equivalent atoms: a = $-x$,1 − y,1−z; b = $-x$,1 − y,$-z$; c = 1 − x,1 − y, 1 − z; d = x,y,$-1+z$; e = $-x$,1 − y,1−z; f = x,1/2−y,$-1/2+z$; g = $-x$,1/2 + y,1/2 − z; h = $-x$,1 − y,1 − z.

[Cg(pyridyl)–Cg(pyridyl): 3.669(3) Å; dihedral angle 1.70(19)] in the *b* direction between adjacent thick 2-D sheets and grow themselves in a zigzag fashion, which favors the AB stacking (figure 5). There also exist interesting interlayer weak N···Cg (2) and S···Cg (1) interactions that stabilize the columnar assembly. The tetrameric supramolecular units are further organized into a 3-D-supramolecular structure (figure 4) in the 010 plane due to the operation of N···π, S···π, and N···N interactions [N4···Cg2^{g}, S1···Cg^{f}, N···N^{h}: 3.325 (4), 3.569 (2), 2.849 f = x,1/2 − y,−1/2 + z; g = −x,1/2 + y,1/2 − z; h = −x,1 − y,1 − z] between N4 and S1 of two oppositely directed SCN^{-} (S1–C11–N4) groups and the other face of the pyridine rings of the particular dpa units. The S1···Cg1, N4···Cg2 distances are 3.569(2) and 3.325(4) Å, respectively, whereas S1 is 3.569 Å and N4 is 3.325 Å vertically above the pyridine ring plane due to a slight miss-alignment of the S1···Cg1 and N4···Cg2 joining line and the ring normal. N···π and S···π interactions are directed along the *b*-axis and the assembly is also extended along the *b*-axis. Involvement of N···π and S···π interactions in supramolecular assembly of

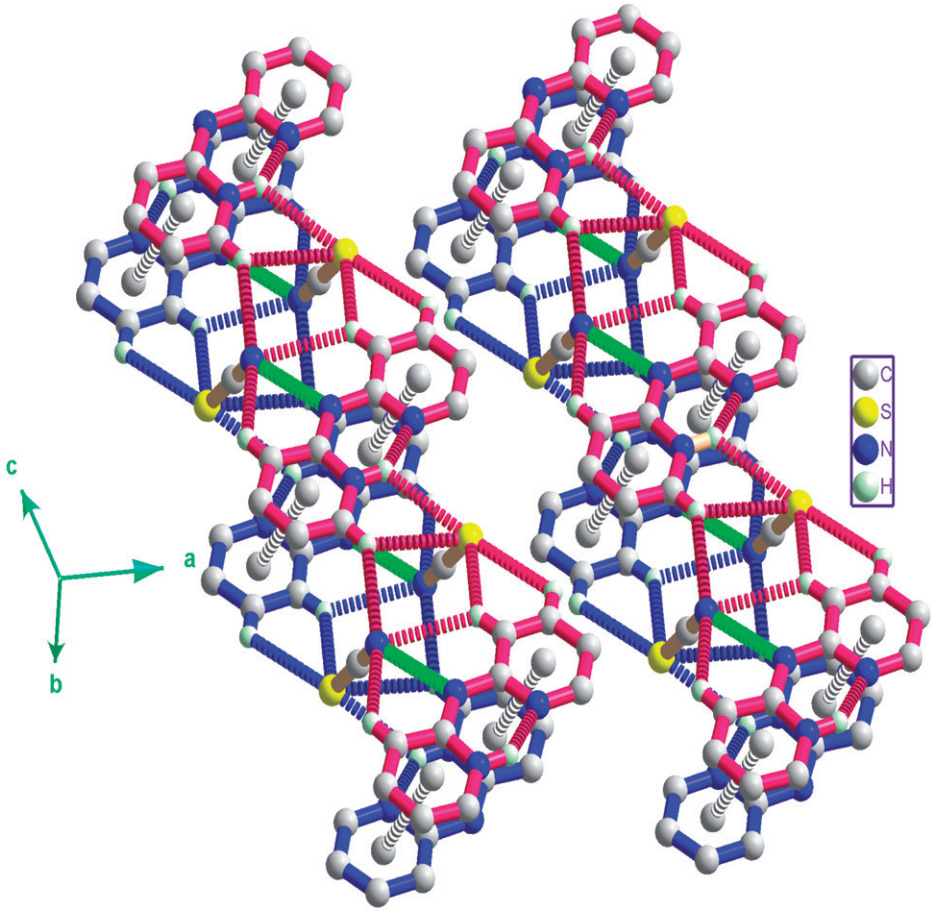

Figure 5. Crystallographic view of AB stacking of adjacent layers (blue and red) in **1** fabricated by different molecular forces like π···π interactions (thick silver broken lines), N/S···H bonds (red and blue broken lines), parallel N···N interactions (green broken lines).

the present salt is noteworthy because this interaction is relatively new and not well explored. The role of S···π and N···π interactions in bio-processes such as protein folding [14a, b] are well established, but its role in the self-assembly of organic/metal organic systems has rarely been explored [21, 22].

The molecular salt assembles into 3-D parallel superstructure (figure 4) due to the influence of the N···N short contacts between successive oppositely faced NCS^- molecular ions. Linear NCS^- ions line up with the help of the N1···N4* interactions (N1···N4* 2.849 Å; $* = -x,1-y,1-z$) giving additional solidity along N4···H1A* H-bond ($* = -x,1-y,1-z$) and form a sheeted assembly along the crystallographic *c*-axis (figure 5). Parallel but oppositely directed NCS^- nodes between the layers communicate intra layers through eight coordination network H-bonds (four each) and N···N short contacts in each sheet of a particular layer leading to 3-D parallel superstructure (figure 4) [23]. Differences in the distances of N···N short contacts at $dpaH^+$ and NCS^- centers is very strong and one of the important cohesive force for the sheeted assembly of the hybrid salt. All coordinate/covalent forces (figure 6) have their own role in controlling the structural assembly and form a hybrid super structure. Selected hydrogen bonding data are summarized in table 2.

3.4. *Anion-sensing study in MeCN solution*

The molecular salt **1** is a simple compound from a structural point of view with receptor adjacent positions being occupied by secondary amine and pyridine rings. Molecular salt **1** exhibits two absorptions at 262 and 308 nm in ACN and also displays an emission maximum at 408 nm when excited at 335 nm in CH_3CN. With increase in the fluoride

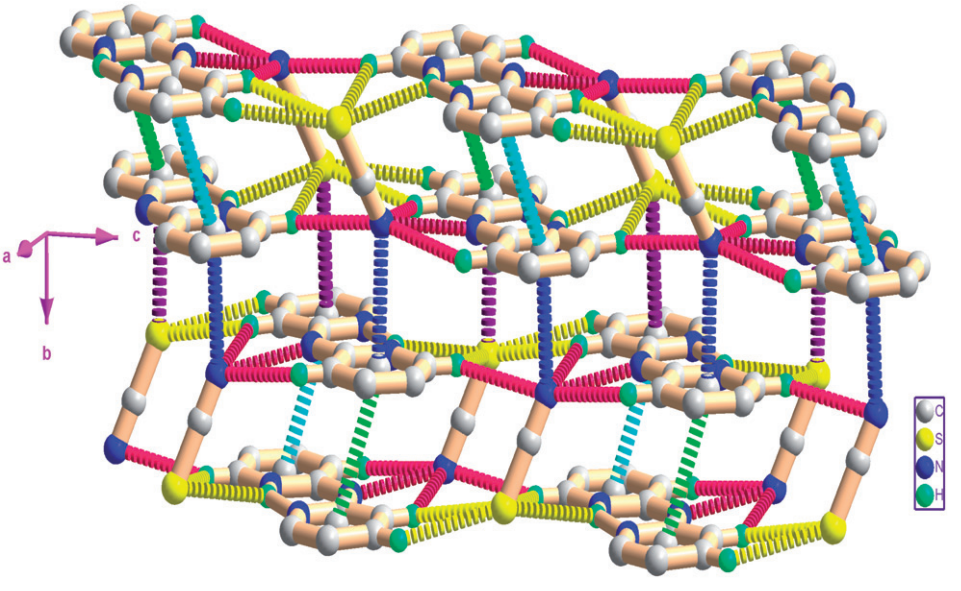

Figure 6. Crystal engineering based on all coordinate/covalent forces present.

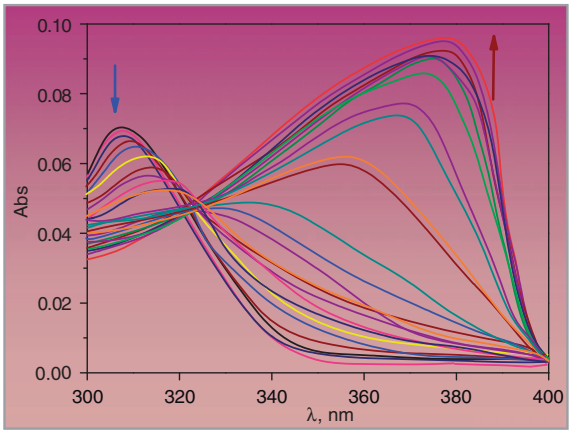

Figure 7. Absorption spectra of **1** in ACN upon the addition of increasing concentrations of fluoride.

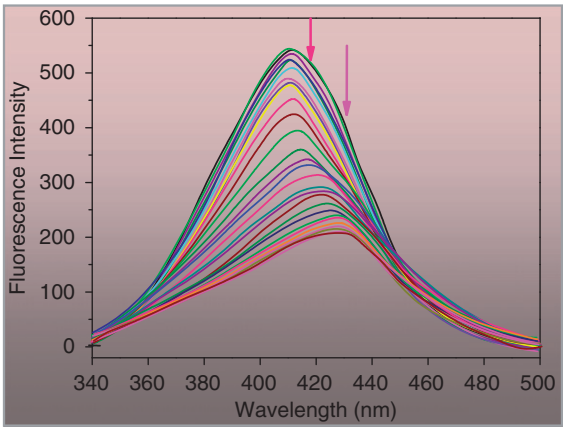

Figure 8. Emission spectra of **1** (50 μM) in ACN in the presence of 10 eqv. of all representative anions ($\lambda_{ex} = 335$ nm).

concentration, a new broad band started to appear around 360–385 nm (figure 7) in absorption and around 408–432 nm (figure 8) in emission spectra, probably due to the absorption of F^- by the salt. The fluorescence measurement clearly shows that fluorescence intensity was quenched and the emission peak red shifted from 408to 432 nm upon the addition of F^-, however, no significant quenching was observed on the addition of other anions. For some receptors, the presence of AcO^- interferes with the detection of F^- [24]. However, in the case of **1** addition of the same amount of AcO^-, as well as other anions such as Cl^-, Br^-, $H_2PO_4^-$, and AcO^-, did not lead to quenching of the fluorescent emission (Supplementary material). The results indicate that **1** is a good sensor for recognizing F^- over other anions. These responses can be exploited, in the ratiometric way, to detect and estimate F^- in micromolar concentrations. These anions were studied as their tetrabutylammonium (TBA) salts.

To verify the anion specificity, some assays have been performed with other tetrabutylammonium salts (TBA–X: X = Cl, Br, CH_3COO, and H_2PO_4). Under

identical experimental conditions the optical response of **1** is practically silent for these anions in spite of large excess compared to fluoride under the same conditions (Supplementary material). Emission spectra of **1** (50 μM) in the presence of equal amounts of all representative anions and relative fluorescence intensity measured at 432 and 408 nm for all the anions are shown in figure 9. These optical results confirm that **1** can detect fluoride selectively. The absorption profile along with the ratiometric chemosensory response can be conveniently used as a fingerprint to discriminate this particular anion. The bands that develop around 432 nm in emission and 381 nm at absorption are due to the protonated form of this molecule and is consistent with the existing literature [25–27]. The plot of the ratio of fluorescence intensity of the two selected bands (figure 10) generates a calibration curve that is independent of the sensor

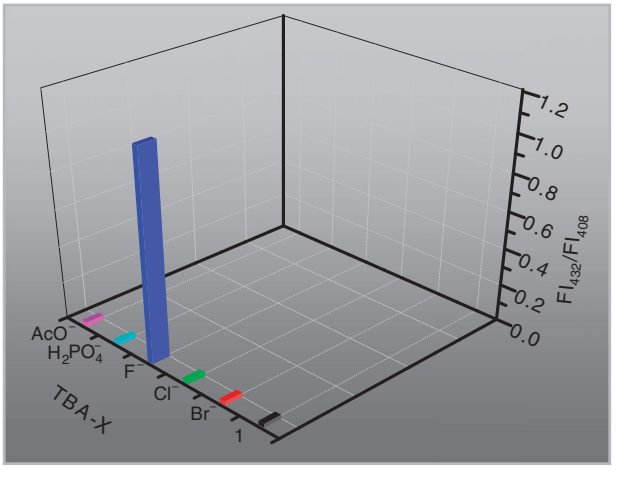

Figure 9. Resultant ratio of fluorescence intensity measured at 432 and 408 nm for each anion ($\lambda_{exe} = 335$ nm).

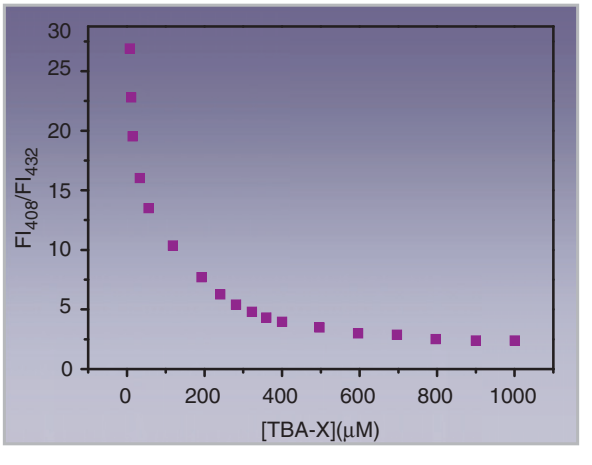

Figure 10. Fluorescence spectrum indicates ratiometric responses by **1** as a function of F^- concentrations.

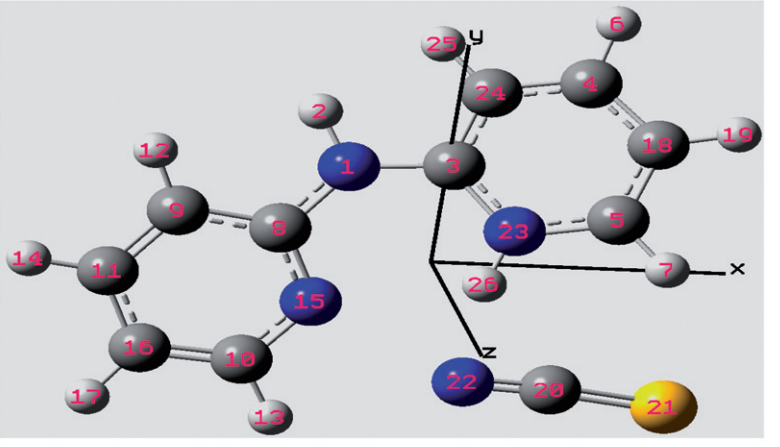

Figure 11. Visualization of the optimized structure of salt **1**.

concentration and allows one to detect and estimate the fluoride present even at micromolar level accurate to 5 mM of the analyte concentration. This ratiometric chemosensory response compares favorably to most sensors known for fluoride [28, 29]. In this particular case for fluoride sensing, hydrogen bonding is the driving force, so only aprotic solvent will be applicable; protic solvents cannot be used. Similar results can be obtained in THF but the sensitivity level is poor compared to ACN. Currently, we are trying to explore these possibilities along with the detailed photophysics, binding, and mechanistic aspects.

3.5. *Geometrical optimization*

The position of the anion and protonated dipyridylamine were fixed so that the distance between the two will be in the approximate range obtained from the crystallographic data before submitting to the Gauss 03 suite of programs and allowing optimization of minimum potential energy. The internal degree of freedom was allowed to relax during the calculation. The optimized geometry showed that the optimized structure was the global minimum on the potential energy surface. In addition to characterization of the salt, the gas phase geometry of the dipyridylamine salt was computed. Comparison of bond lengths and angles of the salts (obtained from theoretical calculation and crystallographic data) are quite similar. The negligible difference in the energy between the optimized structure and crystal structure of these salts suggest that the orientation and interaction remain almost the same in both gaseous and the solid phases (figure 11).

4. Conclusions

We isolated and X-ray crystallographically characterized a molecular salt based on thiocyanate in combination with a symmetrical classical N,N donor chelator through crystal engineering. Though lots of pure organic molecules are available, this classical

hybrid ligand system containing both organic and inorganic donor centers can behave as a new fluorescent chemosensor for fluoride recognition in ACN.

Supplementary material

Crystallographic data are available free of charge from The Director, CCDC, 12 Union Road, Cambridge, CB2 1EZ, UK (Fax: +44-1223-336033; E-mail: deposit@ccdc.cam.ac.uk or www: http://www.ccdc.cam.ac.uk) upon request, quoting deposition number CCDC 830888 for **1**.

Acknowledgments

This work is supported financially by the University Grants Commission (UGC), New Delhi, India, by grant MRP No. F. PSW-039/09-10(ERO) dated 08/10/2009. H.-L. Tsai thanks the National Science Council of Taiwan for financial support under grant No. NSC 99-2113-M-006-003-MY3. B. Biswas sincerely thanks Dr Arabinda Mallick, Kashipur Michael Madhusudan Mahavidyalaya, Purulia, 723132, India, for valuable discussions.

References

[1] Y. Xia, B. Wu, Y. Liu, Z. Yang, X. Huang, L. He, X.J. Yang. *CrystEngComm*., **11**, 1849 (2009).
[2] B. Wu, X. Huang, Y. Xia, X.J. Yang, C. Janiak. *CrystEngComm*., **9**, 676 (2007).
[3] P.S. Lakshminarayanan, I. Ravikumar, E. Suresh, P. Ghosh. *Chem. Commun*., 5214 (2007).
[4] D.A. Jose, D.K. Kumar, B. Ganguly, A. Das. *Inorg. Chem*., **46**, 5817 (2007).
[5] D.A. Jose, P. Kar, D. Koley, B. Ganguly, W. Thiel, H.N. Ghosh, A. Das. *Inorg. Chem*., **46**, 5576 (2007).
[6] A. Ghosh, A. Shrivastav, D.A. Jose, S.K. Mishra, C.K. Chandrakanth, S. Mishra, A. Das. *Anal. Chem*., **8**, 5312 (2008).
[7] (a) G.R. Desiraju. *Angew. Chem., Int. Ed. Engl*., **34**, 2311 (1995); (b) B. Moulton, M.J. Zaworotko. *Chem. Rev*., **101**, 1629 (2001); (c) B. Moulton, M.J. Zaworotko. In *Perspective in Supramolecular Chemistry: The Crystal as a Supramolecular Entity*, G.R. Desiraju (Ed.), Vol. 2, pp. 137–233, John Wiley & Sons Ltd., Chichester (1996); (d) J.M. Lehn. *Supramolecular Chemistry: Concepts and Perspectives*, VCH, Weinheim (1995).
[8] S.R. Seidel, P.J. Stang. *Acc. Chem. Res*., **35**, 972 (2002).
[9] (a) G.A. Jeffrey. *An Introduction to Hydrogen Bonding*, Oxford University Press, Oxford (1997); (b) G.R. Desiraju, T. Steiner. *The Weak Hydrogen Bond in Structural Chemistry and Biology*, Oxford University Press, Oxford (1999).
[10] (a) C. Janiak. *Angew. Chem*., *Int. Ed. Engl*., **36**, 1431 (1997); (b) K.M. Detlefs, P. Hobza. *Chem. Rev*., **100**, 143 (2000).
[11] (a) M. Nishio, M. Hirota, Y. Umezawa. *The CH/p Interaction*, Wiley-VCH, New York (1998); (b) H. Takahashi, S. Tsuboyama, Y. Umezawa, K. Honda, M. Nishio. *Tetrahedron*, **56**, 6185 (2000).
[12] (a) L. Cronin, S.J. Clark, S. Parsons, T. Nakamura, N. Robertson. *J. Chem. Soc*., *Dalton Trans*., 1347 (2001); (b) D.B. Leznoff, B.-Y. Xue, R.J. Batchelor, F.W.B. Einstein, B.O. Patrick. *Inorg. Chem*., **40**, 6026 (2001).
[13] (a) M. Munakata, T. Kuroda-Sowa, M. Maekawa, A. Hirota, S. Kitagawa. *Inorg. Chem*., **34**, 2705 (1995); (b) A.D. Bond, D.A. Haynes, C.M. Pask, J.M. Rawson. *J. Chem. Soc., Dalton Trans*., 2522 (2002).
[14] (a) R. Bhattacharyya, D. Pal, P. Chakrabarti. *Protein Eng. Des. Selection*, **17**, 795 (2004); (b) R.K. Castellano, F. Diederich, E.A. Meyer. *Angew. Chem*., *Int. Ed*., **42**, 1210 (2003).

[15] L.K. Haas, J.K. Franz. *Chem. Rev*., **109**, 4921 (2009).
[16] H.D.P. Ali, P.E. Kruger, T. Gunnlaugsson. *New J. Chem*., **32**, 1153 (2008).
[17] *SHELXTL 5.10*. Bruker Analytical X-ray Instruments Inc., Karlsruche, Germany (1997).
[18] L.J. Farrugia. *J. Appl. Crystallogr*., **30**, 565 (1997).
[19] (a) K. Nakamoto. *Infrared and Raman Spectra of Inorganic and Coordination Compounds Part B: Applications in Coordination, Organometallic and Bioinorganic Chemistry*, John Wiley & Sons Inc., New York (1997); (b) B. Stuart. *Infrared Spectroscopy: Fundamentals and Applications*, Wiley, New York (2004); (c) C.N.R. Rao, V. Sampathkumaran, R. Nagarajan, G. Paul, J.N. Behra, A. Choudhury. *Chem. Mater*., **16**, 1441 (2004).
[20] J.G. Sole, L.E. Bausa, D. Jaque. *An Introduction to Optical Spectroscopy of Inorganic Solids*, John Wiley & Sons Ltd., New York (2005).
[21] A.D. Jana, S.C. Manna, G.M. Rosair, M.G.B. Drew, G. Mostafa, N.R. Chaudhuri. *Cryst. Growth Des*., **7**, 1365 (2007).
[22] M.C. Aragoni, M. Arca, M. Crespo, F.A. Devillanova, M.B. Hursthouse, L.S. Huth, F. Isaia, V. Lippolisa, G. Verania. *CrystEngComm*., **9**, 873 (2007).
[23] R. Ghosh, A.D. Jana, S. Pal, G. Mostafa, H.K. Fun, B.K. Ghosh. *CrystEngComm*., **9**, 353 (2007).
[24] J.V. Ros-Lis, R. Martínez-Máñez, F. Sancenón, J. Soto, K. Rurack, H. Weißhoff. *Eur. J. Org. Chem*., 2449 (2007).
[25] A. Chakrabarty, A. Mallick, P. Purkayastha, B. Haldar, N. Chattopadhyay. *Langmuir*, **23**, 4842 (2007).
[26] A. Chakrabarty, A. Mallick, P. Das, B. Haldar, N. Chattopadhyay. *Biomacromolecules*, **8**, 920 (2007).
[27] A. Chakrabarty, A. Mallick, P. Das, N. Chattopadhyay. *J. Phys. Chem. B*, **112**, 3684 (2008).
[28] C.I. Lin, S. Selvi, J.-M. Fang, P.T. Chou, C.-H. Lai, Y.-M. Cheng. *J. Org. Chem*., **72**, 3537 (2007).
[29] M. Vazquez, L. Fabbrizzi, A. Taglietti, R.M. Pedrido, A.M. Gonzalez-Noya, M.R. Bermejo. *Angew. Chem., Int. Ed*., **43**, 1962 (2004).